Supplementary Information

Scale-up of Complex Molecular Reaction System by Hybrid Mechanistic Modeling and Deep Transfer Learning

Zhengyu Chen[1], Yongqing Xie[1], Chunming Xu[1], and Linzhou Zhang[1]*

[1]*State Key Laboratory of Heavy Oil Processing, Petroleum Molecular Engineering Center (PMEC), China University of Petroleum, Beijing, 102249, P. R. China*

*Corresponding Author Email: Lzz@cup.edu.cn (Linzhou Zhang)

Contents

Supplementary Note 1. Detailed PIONA composition of naphtha used in this work

Supplementary Table 1. Detailed PIONA composition of naphtha[1]

Carbon number	3	4	5	6	7	8	9	10	11	12	13	Total
Naphtha 1, wt%												
n-Paraffins		0.55	0.92	1.14	1.03	1.05	0.28	0.25	0.2	0.18		5.6
i-Paraffins		1.04	5.27	8.39	5.52	3.29	1.74	1.23	0.9	0.11	0.19	27.68
Olefins	0.23	3.07	8.69	10.95	7.97	4.41	1.35	1.09	0.07			37.83
Naphthenes			0.08	0.23	4.11	1.13	0.53	0.15	0	0.07		6.3
Aromatics				0.25	3.1	7.29	6.22	4.39	1.34			22.59
Naphtha 2, wt%												
n-Paraffins		0.4	0.8	1	1	1.2	0.4	0.4	0.2	0.1	0.1	5.6
i-Paraffins		0.7	3.9	6.3	5	3.9	1.9	1.9	1.1	0.3	0.3	25.3
Olefins	0.2	2.4	6.9	9.3	9	5.9	2.8	2.2	0.2			38.9
Naphthenes			0.1	0.2	3.5	1.4	1.3	0.3	0.1	0.1		7
Aromatics					3.1	7.6	6.1	4.9	1.5			23.2
Naphtha 3, wt%												
n-Paraffins		0.5	0.7	0.8	0.9	1.1	0.3	0.2	0.1			4.6
i-Paraffins		1	4	5.9	3.3	2.9	1.5	2.1	0.8	0.1	0.1	21.7
Olefins	0.1	4.3	10.7	12.5	10.6	6.4	3.6	1.7	0.1			50
Naphthenes			0.1	0.2	3.2	1.4	2.9	0.5				8.3
Aromatics					2.2	4.8	5.3	2.7	0.4			15.4

Supplementary Note 2. Reaction rules for naphtha FCC

Supplementary Table 2. Reaction rules for naphtha FCC

Reaction family	Representative reaction	Reaction family	Representative reaction
n-Paraffin cracking	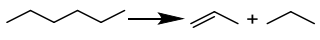	i-Paraffin cracking	
Paraffin cracking to C1C2	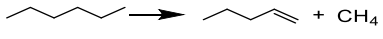	Ring side chain cracking	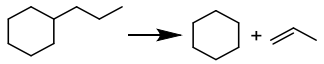
Paraffin isomerization	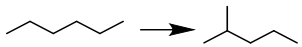		
Olefin cracking	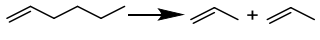	Olefin isomerization	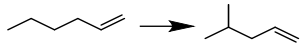
Hydrogen transfer 4H	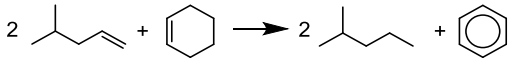	Hydrogen transfer 6H	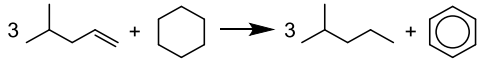
Aromatic alkylation	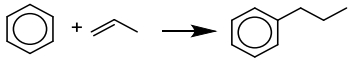	Paraffin alkylation	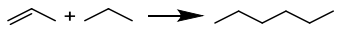
Olefin polymerization	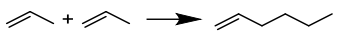	Olefin ring closure	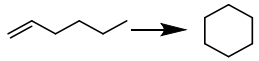
Paraffin dehydrogenation	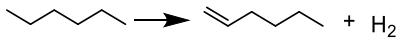	Naphthenic ring dehydrogenation 2H	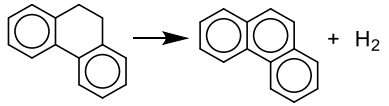
Naphthenic ring dehydrogenation 4H	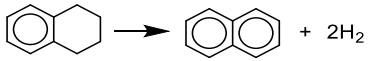	Naphthenic ring dehydrogenation 6H	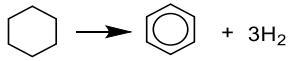
Ring condensation 2H	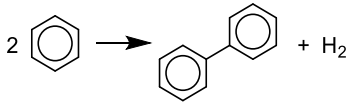	Ring condensation 6H	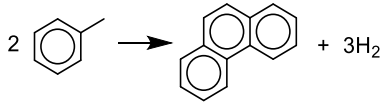

Supplementary Note 3. Model parameter organization via LFER and QSRC

The Langmuir-Hinshelwood-Hougen-Watson (LHHW) equation was used to calculate the reaction rate of each molecule, as shown in Eqs. (S1) and (S2).

$$r_j = \frac{k_j K_{\mathrm{ads}_A} K_{\mathrm{ads}_B} \left(C_A^p C_B^q\right)}{1 + \sum K_{\mathrm{ads}_i} C_i} \tag{S1}$$

$$k_j = A_j \mathrm{e}^{-\frac{\mathrm{Ea}_j}{\mathrm{R}T}} \tag{S2}$$

There are a large number of kinetic parameters for the complex molecular reaction system. The linear free energy relationship (LFER) and the quantitative structure-reactivity correlations (QSRCs) were employed to organize the model parameters, as shown in Eqs. (S3) ~ (S5).

$$\mathrm{Ea}_j = E_{0_n} - \alpha_n \times \Delta H_j \tag{S3}$$

$$\mathrm{Ea}_j = E_{0_n} - (1 - \alpha_n) \times \Delta H_j \tag{S4}$$

$$\ln K_{\mathrm{ads}_i} = a + \frac{\left(bN_{\mathrm{AR}_i} + cN_{\mathrm{SC}_i}\right)}{\mathrm{R}T} \tag{S5}$$

The LFER assumes a linear relationship between activation energy and enthalpy change for reactions from the same reaction family, as shown in Eqs. (S3) and (S4). In this work, the enthalpy change was calculated using the group contribution method. α_n and E_{0_n} are regressed parameters, and reactions from the same reaction family share the same α_n and E_{0_n}. Moreover, Eq. (S3) was utilized to compute the activation energy of exothermic reactions, while Eq. (S4) was used to estimate the activation energy of endothermic reactions.

The adsorption constant of each species can be calculated by molecular physics structure, such as the number of aromatic rings and naphthenic carbon number, as shown in Eq. (S5). In Eq. (S5), a, b, and c were parameters required to be fitted by the experimental data.

Supplementary Note 4. Impurity and catalyst deactivation in the mechanistic model

In the naphtha FCC process, coke is a critical impurity. It is both a by-product and a contaminant. It is mainly composed of polycyclic aromatic hydrocarbons (PAHs) and forms through the dehydrogenation and condensation reactions of aromatics in the feedstock. Once formed, coke readily deposits on the active sites of the catalyst, leading to catalyst deactivation.

In the mechanistic model, the formation pathway of coke and its impact on catalytic activity were detailed described. The reaction pathways of coke formation were generated by reaction rules for ring condensation, as listed in Supplementary Table 2, and detailed reaction pathways are provided in Supplementary Data 1 and 2.

Moreover, catalyst deactivation was explicitly considered in the development of the laboratory-scale mechanistic model and incorporated into the mass balance equation, as shown in Eqs. (S6) and (S7). Eq. (S6) represents the mass balance, and Eq. (S7) describes catalyst deactivation caused by coke deposition on the catalyst surface.

$$\frac{\mathrm{d}C_i}{\mathrm{d}X} = \frac{P\mathrm{Mw}}{\mathrm{SwR}T} r_i \varphi_\mathrm{c} \tag{S6}$$

$$\varphi_\mathrm{c} = (1 + \alpha C_\mathrm{C})^{-\beta} \tag{S7}$$

In Eq. (S7), φ_c is the deactivation factor, and C_C represents the coke content per unit mass of catalyst and can be calculated using Eq. (S8). Model parameters (α and β) were previously determined through regression of experimental data and have values of 0.48 and 1.4, respectively.[1] These parameters are intrinsic to the catalyst and remain constant across reactor scales.

$$C_\mathrm{C} = \frac{w_\mathrm{coke} \cdot m_\mathrm{oil}}{m_\mathrm{cat}} = \frac{w_\mathrm{coke}}{\mathrm{CTO}} \tag{S8}$$

Substituting Eq. (R8) into Eq. (R7), the effect of coke on catalytic activity can be quantitatively estimated. This relationship is visualized in Supplementary Fig. 1.

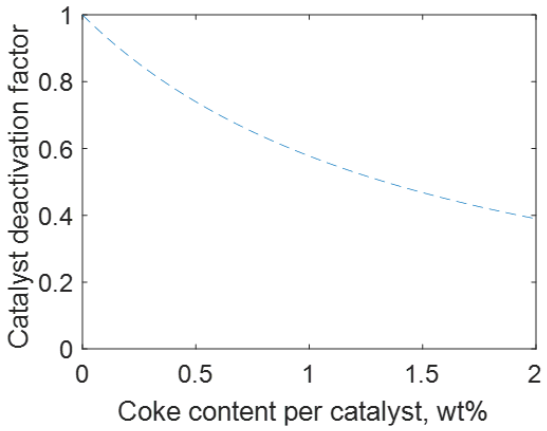

Supplementary Fig. 1. The effect of coke content on reaction rate. Source data are provided as a Source Data file.

Because the mechanistic model included detailed formation information for coke impurities, it ensures that the pilot-scale hybrid model trained on this mechanistic data can also accurately calculate the distribution of coke. Figs. 5 and 8 present the predicted coke content under various process conditions and feedstock compositions, demonstrating that the hybrid model effectively captured the relationship between molecular feed characteristics and coke formation.

Supplementary Note 5. Kinetic parameters for laboratory-scale naphtha FCC

Supplementary Table 3. Kinetic parameters for laboratory-scale naphtha FCC

Reaction family	A	Ea, kJ/mol
n-Paraffin cracking	$3.38*10^{0}$	101.95
i-paraffin cracking	$6.12*10^{5}$	68.01
Olefin cracking	$1.73*10^{6}$	75.39
Ring side chain cracking	$7.96*10^{5}$	77.32
Paraffin cracking to C1C2	$3.37*10^{7}$	121.32
Paraffin isomerisation	$1.37*10^{5}$	52.95
Olefin isomerisation	$4.25*10^{6}$	60.34
Hydrogen transfer 4H	$3.61*10^{1}$	45.6
Hydrogen transfer 6H	$1.21*10^{6}$	51.2
Aromatic alkylation	$2.63*10^{3}$	45.76
Paraffin alkylation	$1.00*10^{5}$	47.85
Olefin polymerization	$5.64*10^{4}$	45.3
Olefin ring closure	$1.03*10^{8}$	66.5
Paraffin dehydrogenation	$1.03*10^{3}$	25.86
Naphthenic ring dehydrogenation 2H	$7.52*10^{2}$	43.53
Naphthenic ring dehydrogenation 4H	$5.53*10^{2}$	53.53
Naphthenic ring dehydrogenation 6H	$8.85*10^{3}$	20.07
Ring condensation 2H	$7.90*10^{3}$	32.95
Ring condensation 6H	$9.05*10^{1}$	0

Supplementary Note 6. Hyperparameter optimization results for laboratory-scale hybrid model based on various metrics

Supplementary Table 4. Hyperparameter optimization results for laboratory-scale hybrid model based on various metrics

Hyperparameter	R^2	MAE	RMSE	likelihood
Training set R^2	0.956	-2.32	0.955	0.55
Testing set R^2	0.953	-2.99	0.952	0.56
Training set MAE	$7.23*10^{-5}$	$7.08*10^{-5}$	$8.21*10^{-5}$	$3.92*10^{-4}$
Testing set MAE	$7.75*10^{-5}$	$7.61*10^{-5}$	$8.69*10^{-5}$	$3.88*10^{-4}$
Training set MSE	$3.85*10^{-8}$	$3.13*10^{-8}$	$5.61*10^{-8}$	$1.45*10^{-6}$
Testing set MSE	$4.33*10^{-8}$	$3.58*10^{-8}$	$6.24*10^{-8}$	$1.41*10^{-6}$
	Hyperparameter			
Residual block number for process-based ResNet	2	2	2	1
Residual block number for molecule-based ResNet	2	2	1	1
Residual block number for integrated ResNet	3	2	4	1
Neuron number for process-based ResNet	128	512	128	256
Neuron number for molecule-based ResNet	512	512	256	512
Neuron number for integrated ResNet	256	1024	1024	512
Learning rate	$3.47*10^{-5}$	$1.63*10^{-5}$	$9.12*10^{-5}$	$1.08*10^{-5}$
Dropout parameter	0.14	0.01	0.01	0.03
Weight decay	$1.61*10^{-6}$	$1.20*10^{-6}$	$1.02*10^{-6}$	$2.49*10^{-4}$
Batch size	16	32	16	16
Epoch number	300	300	300	300

We evaluated different metrics as the objective function for the BO algorithm. During the optimization process, the same upper and lower bounds for hyperparameters were applied, with the number of optimization trials set to 100. The optimal results are presented in Supplementary Table 4. Although using MAE as the objective function resulted in the lowest error, its corresponding R^2 score is relatively poor. After a comprehensive comparison of the optimization results in Supplementary Table 4, R^2 was selected as the objective function of the BO algorithm to ensure both accuracy and overall model reliability.

Supplementary Note 7. Optimal ResNet architecture of hybrid model by BO algorithm

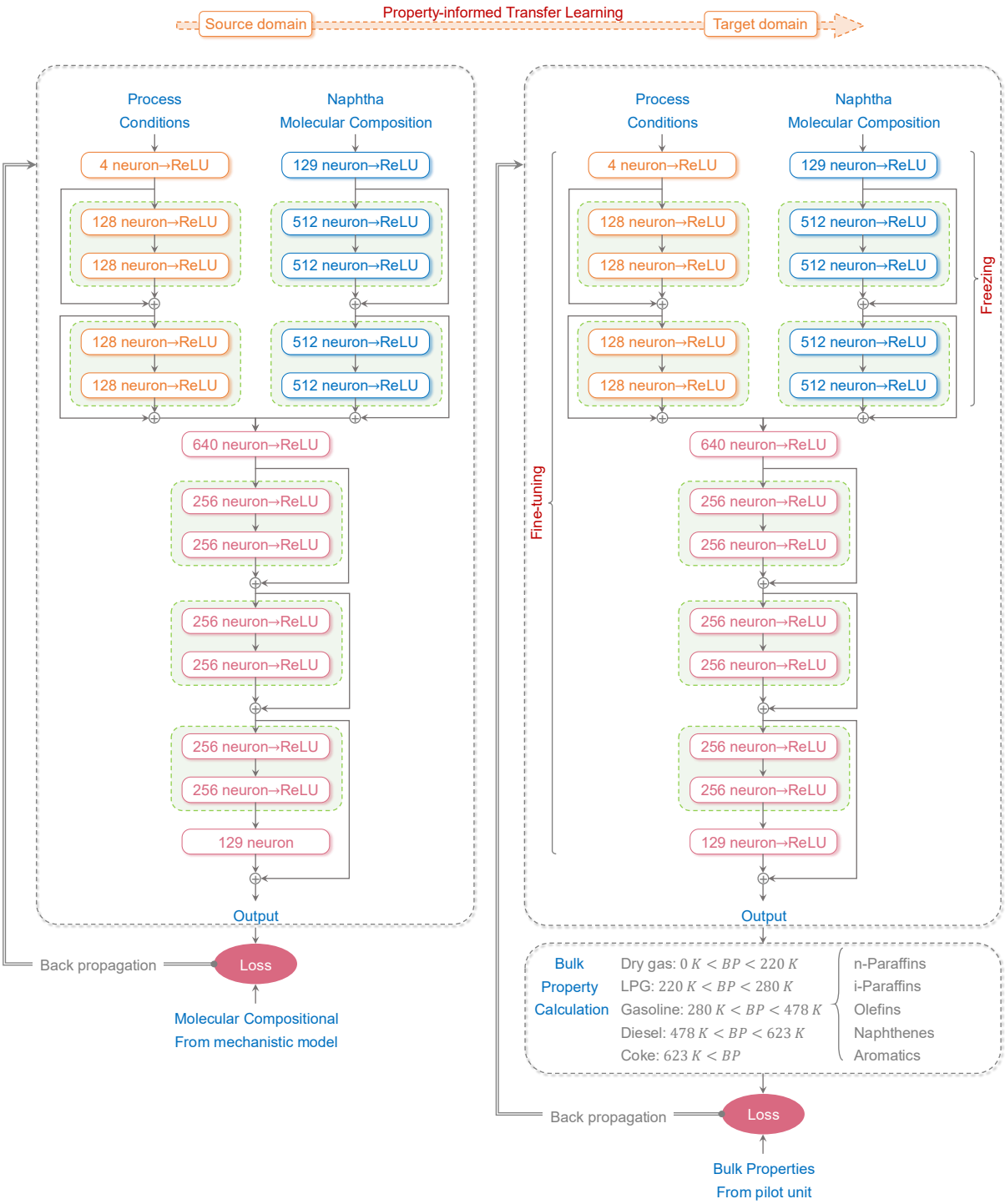

Supplementary Fig. 2. Optimal ResNet architecture of hybrid model by BO algorithm.

Supplementary Note 8. Training results for various neural network structures

We compared the training results of various neural network structures, as shown in Supplementary Table 5. All hyperparameters in the neural network were optimized using the Bayesian optimization algorithm, with the number of optimization iterations set to 100. Compared to the training results of the single neural network, the network structures proposed by this work can obtain better training performance.

Supplementary Table 5. Training results for various neural network structures

	This work	Single ResNet	Single neural network
Training set R^2	0.956	0.912	0.737
Testing set R^2	0.953	0.910	0.736
Training set MAE	$7.23*10^{-5}$	$1.13*10^{-4}$	$2.80*10^{-4}$
Testing set MAE	$7.75*10^{-5}$	$1.15*10^{-4}$	$2.78*10^{-4}$
Training set MSE	$3.85*10^{-8}$	$9.44*10^{-8}$	$7.43*10^{-7}$
Testing set MSE	$4.33*10^{-8}$	$9.50*10^{-8}$	$7.27*10^{-7}$
		Hyperparameter	
Block/Layer number	2/2/3	4	2
Neuron number	128/512/256	256	1st layer: 128 2nd layer:256
Learning rate	$3.47*10^{-5}$	$2.04*10^{-5}$	$1.22*10^{-5}$
Dropout parameter	0.14	0.27	0.15
Weight decay	$1.61*10^{-6}$	$7.11*10^{-6}$	$4.64*10^{-6}$
Batch size	16	16	16
Epoch number	300	300	300

Note: x/x/x corresponds to Process-based ResNet, Molecule-based ResNet, and Integrated ResNet, respectively.

Supplementary Note 9. Comparison of calculated results between hybrid model and mechanistic model

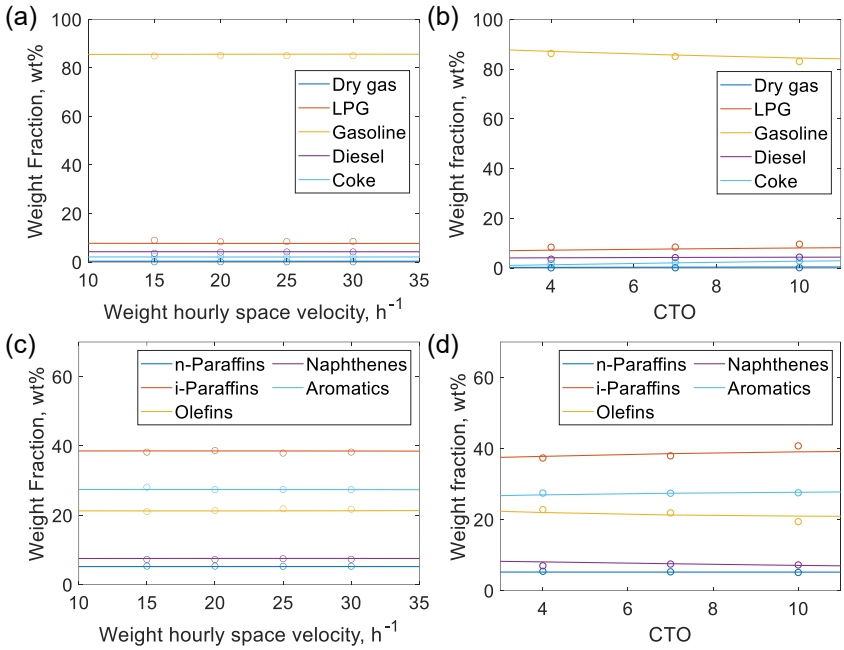

Supplementary Fig. 3. Comparison of calculated results between hybrid model and mechanistic model. (a) Effect of WHSV on the product fractions; (b) Effect of CTO on the product fractions; (c) Effect of WHSV on the gasoline composition; (d) Effect of CTO on the gasoline composition. Source data are provided as a Source Data file.

Supplementary Note 10. Transfer learning hyperparameters for various datasets

Supplementary Table 6. Transfer learning hyperparameters for various datasets

Hyperparameter	980	750	500	250	100	80	60	50	40
Learning rate	$6.48*10^{-6}$	$7.31*10^{-6}$	$8.49*10^{-6}$	$9.38*10^{-6}$	$8.44*10^{-5}$	$8.78*10^{-6}$	$1.22*10^{-5}$	$9.14*10^{-6}$	$1.60*10^{-5}$
Dropout parameter	0.13	0.14	0.08	0.18	0.19	0.40	0.15	0.38	0.18
Weight decay	$4.91*10^{-4}$	$1.47*10^{-4}$	$8.08*10^{-6}$	$3.56*10^{-5}$	$7.51*10^{-4}$	$4.22*10^{-4}$	$3.48*10^{-4}$	$1.33*10^{-4}$	$4.01*10^{-6}$
Batch size	16	16	16	16	16	4	4	4	4
Epoch number	300	300	300	300	300	300	300	300	300

Supplementary Note 11. Pilot-scale product yield over time

Prediction of product distribution over time by the developed model is significant for understanding the reaction progress and optimizing the process conditions. Thus, this work compared the product distribution profiles calculated by the hybrid model and the mechanistic model. A pilot-scale molecular-level mechanistic model for naphtha FCC was developed, which allowed us to generate product data at different time intervals. Details on the pilot-scale mechanistic model were introduced in Supplementary Note 13. The transfer learning strategy presented in this study was then applied to fine-tune the neural network using the generated time-series data. The tuned results and hyperparameters are shown in Supplementary Table 7. Additionally, the product distribution over time predicted by the hybrid model and the mechanistic model was compared in Supplementary Fig. 4. In this figure, lines represent predictions from the hybrid model, while points denote mechanistic model calculations. The predicted results from the hybrid model show excellent agreement with the mechanistic model, demonstrating the ability of the proposed architecture to capture product variation over time.

Supplementary Table 7. Fine-tuned results based on time-series product data

Metrics	Value	Hyperparameter	Value
Training set MAE	0.03	Block/Layer number	2/2/3
Testing set MAE	0.08	Neuron number	128/512/256
Training set MSE	0.01	Learning rate	$1.93*10^{-5}$
Testing set MSE	0.01	Dropout parameter	0.25
		Batch size	8
		Epoch number	300
		Weight decay	$4.03*10^{-6}$

Note: x/x/x corresponds to process-based ResNet, molecule-based ResNet, and integrated ResNet, respectively.

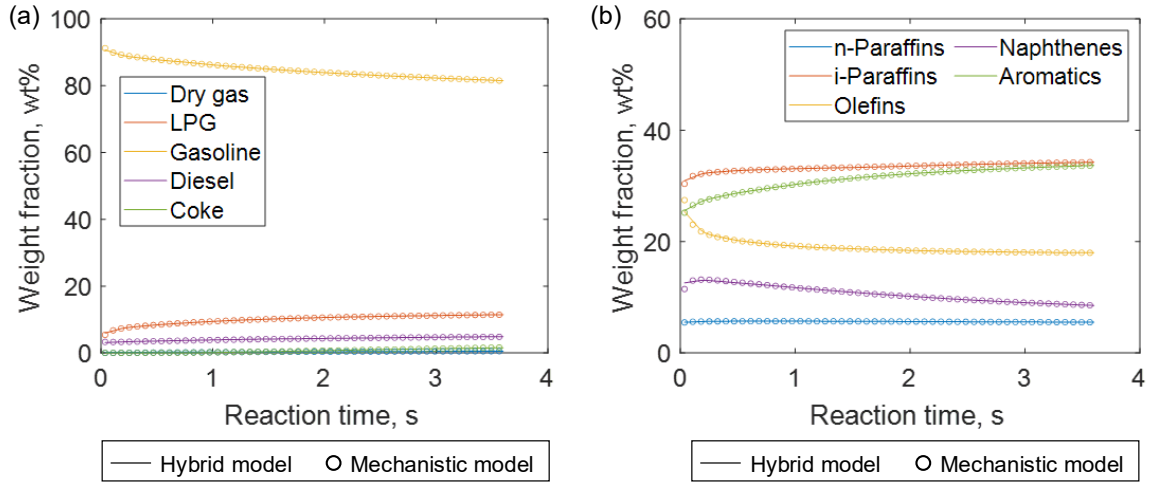

Supplementary Fig. 4. Predicted pilot-scale product distribution over time. (a) Fraction yield; (b) Gasoline composition. Source data are provided as a Source Data file.

Supplementary Note 12. Partial temperature control for FCC pilot-scale plant

1. Feed Temperature Control

The feedstock temperature is regulated by adjusting the flow rate of the heat carrier in the preheater. A temperature indicator (TI) is installed at the preheated naphtha pipe to monitor the feed temperature. A control valve is installed at the inlet of the heat carrier. On this basis, a temperature indicating controller (TIC) was used to adjust the valve opening, increasing the feed temperature by 8°C, as illustrated in Supplementary Fig. 5.

2. Regenerated Catalyst Temperature Control

The regenerated catalyst temperature is related to the reaction temperature in the regenerator. To regulate the regenerated catalyst temperature, we intend to control the reaction temperature in the regenerator by changing the air flow at the regenerator inlet. A temperature indicator (TI) is installed on the sloped pipe of the regenerated catalyst to monitor the catalyst temperature, while a control valve is placed at the air pipe. Then, a temperature indicating controller (TIC) was used to adjust the valve opening to reduce the air flow rate, reducing the regenerated catalyst temperature by 8°C, as shown in Supplementary Fig. 5.

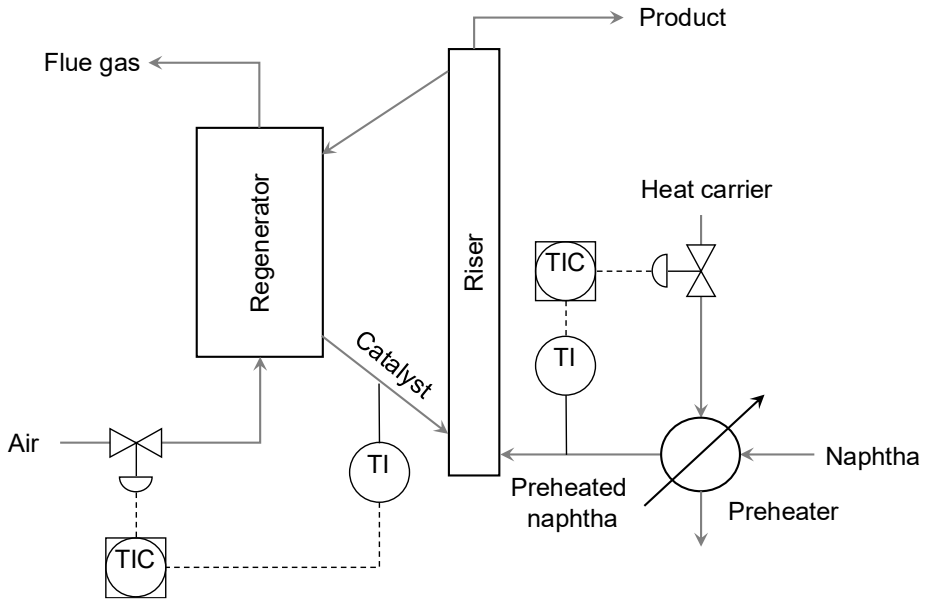

Supplementary Fig. 5. Control structure for feedstock temperature and regenerated catalyst temperature

Supplementary Note 13. Molecular-level mechanistic model for pilot-scale plant

To validate the optimization results of NN-NSGA, we developed a molecular-level mechanistic model for pilot-scale naphtha FCC. Compared to the laboratory-scale FCC model, the pilot-scale FCC model requires integrating the molecular-level kinetic model with the riser reactor model. The mass and heat balance equations in the riser model are presented in Eqs. (S9) ~ (S11).

$$\frac{\mathrm{d}C_i}{\mathrm{d}z} = \frac{\rho_\mathrm{c}\varepsilon_\mathrm{c}}{v_\mathrm{g}} R_i \varphi_\mathrm{ck} \tag{S9}$$

$$\frac{\mathrm{d}T_\mathrm{c}}{\mathrm{d}z} = \frac{A h_\mathrm{p} A_\mathrm{p}}{F_\mathrm{c} C_\mathrm{pc}} \left(T_\mathrm{g} - T_\mathrm{c}\right) \tag{S10}$$

$$\frac{\mathrm{d}T_\mathrm{g}}{\mathrm{d}z} = \frac{A}{F_\mathrm{g} C_\mathrm{pg}} \left[h_\mathrm{p} A_\mathrm{p} \left(T_\mathrm{c} - T_\mathrm{g}\right) + \rho_\mathrm{c}\varepsilon_\mathrm{c} \sum\nolimits_j \left(-\Delta H_j r_j\right) \right] \tag{S11}$$

The mass and heat balance equations in the riser reactor model involve numerous bulk properties, and their correlation formulas are shown in Supplementary Table 8. After developing the molecular-level kinetic model for the naphtha FCC, the kinetic parameters were regressed using pilot-scale data. The developed model accurately calculated and predicted the product distribution for the pilot-scale unit, as shown in Supplementary Fig. 6.[2]

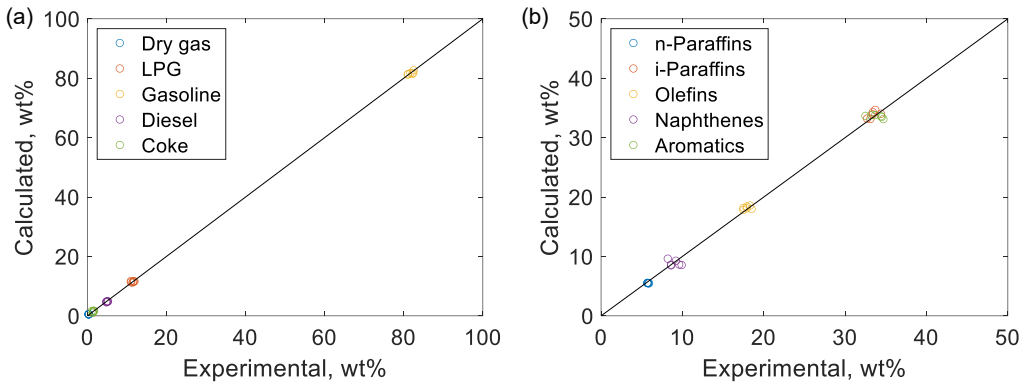

Supplementary Fig. 6. Calculated results for Pilot-scale mechanistic model (a) Product yield; (b) Gasoline composition[2]

Supplementary Table 8. Equations for properties in the riser model

Property	Equations	
Volume fraction for catalyst phase	$\varepsilon_{\mathrm{c}} = \frac{F_{\mathrm{c}}}{v_{\mathrm{c}}\rho_{\mathrm{c}}A}$	(S12)
Volume fraction for oil phase	$\varepsilon_{\mathrm{g}} = 1 - \varepsilon_{\mathrm{c}}$	(S13)
Heat transfer coefficient	$h_{\mathrm{p}} = 0.03\frac{K_{\mathrm{g}}}{d_{\mathrm{c}}^{2/3}}\left[\frac{\left\|\left(v_{\mathrm{g}} - v_{\mathrm{c}}\right)\right\|\rho_{\mathrm{g}}\varepsilon_{\mathrm{g}}}{\mu_{\mathrm{g}}}\right]^{1/3}$	(S14)
Heat transfer area	$A_{\mathrm{p}} = \left(1 - \varepsilon_{\mathrm{g}}\right)\frac{6}{0.72d_{\mathrm{c}}}$	(S15)
Density for oil stream	$\rho_{\mathrm{g}} = \frac{F_{\mathrm{g}}}{\varepsilon_{\mathrm{g}}v_{\mathrm{g}}A}$	(S16)
Heat conductivity	$K_{\mathrm{g}} = 1 \times 10^{-6}\left(1.9469 - 0.374\mathrm{Mw} + 1.4815 \times 10^{-3}\mathrm{Mw}^2 + 0.1028T_{\mathrm{g}}\right)$	(S17)
Oil viscosity	$\mu_{\mathrm{g}} = 3.515 \times 10^{-8}\mu_{\mathrm{pr}}\frac{\sqrt{\mathrm{Mw}P_{\mathrm{pc}}^{2/3}}}{T_{\mathrm{pc}}^{1/6}}$	(S18)
Pseudo-reduced viscosity	$\mu_{\mathrm{pr}} = 0.435\exp\left[\left(1.3316 - T_{\mathrm{pr}}^{0.6921}\right)P_{\mathrm{pr}}\right]T_{\mathrm{pr}} + 0.0155$	(S19)
Pseudo-reduced pressure	$P_{\mathrm{pr}} = \frac{P}{P_{\mathrm{pc}}}$	(S20)
Pseudo-reduced temperature	$T_{\mathrm{pr}} = \frac{T_{\mathrm{g}}}{T_{\mathrm{pc}}}$	(S21)

Supplementary Note 14. The uncertainty in the hybrid model

The developed hybrid model has uncertainties in experimental data, mechanistic models, and hybrid models. The specific discussion is as follows:

1. Experimental data: The product composition analysis for both laboratory-scale and pilot-scale units relied on offline analytical methods, introducing uncertainties in experimental data acquisition. Additionally, the composition of feedstock and product fraction was analyzed using a GC-FID, following the ASTM D5134-21 standard method. The uncertainty of this analytical method is less than ± 0.01 (mass fraction). The FCC products are separated using a micro distillation device, and the uncertainty is less than 1 mL.

2. Mechanistic model: The molecular-level kinetic model developed in this work decomposed reversible reactions into two irreversible reactions, which may introduce deviations in the generated molecular conversion data.

3. Hybrid model: The developed neural network may introduce uncertainties when calculating product distributions outside the boundary process conditions.

Supplementary Note 15. Process parameters of laboratory-scale and pilot-scale reactors

Supplementary Table 9. Main process parameters of laboratory-scale and pilot-scale reactors

Parameter	Data
Fixed fluidized bed reactor	
Reactor volume, cm^3	600
Reactor diameter at top, cm	5.5
Reactor height, cm	41
Catalyst loading, g	150
Riser	
Riser length, cm	665
Riser diameter, cm	1.6
Mass flow rate for feedstock, kg/h	2
Mass flow rate of atomizing steam, kg/h	0.3
Pressure, kPa	135
Pressure drop, kPa	2.64

Supplementary Note 16. Laboratory-scale reactor and experiment scheme for naphtha FCC

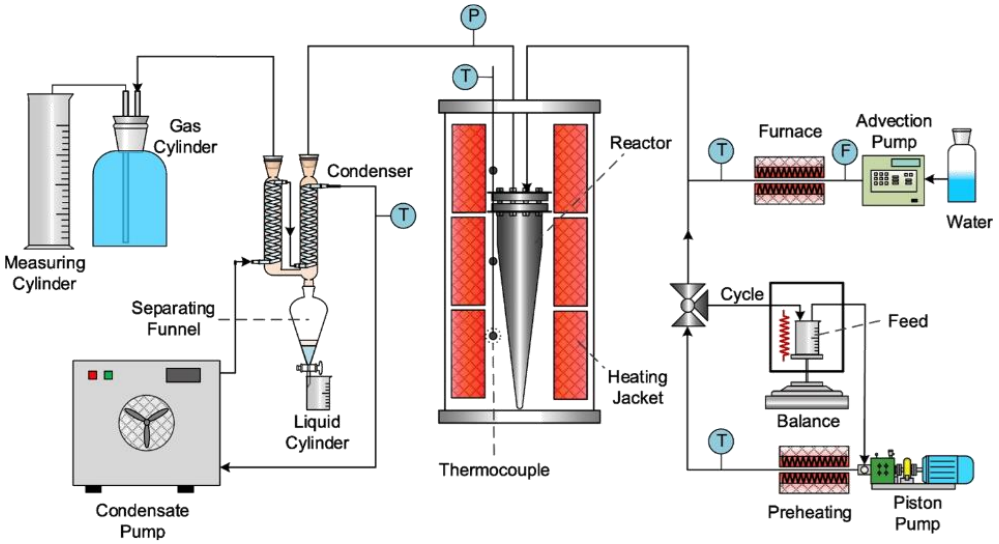

Supplementary Fig. 7. Laboratory-scale reactor and experiment scheme for naphtha FCC

Supplementary Note 17. Catalyst properties for laboratory-scale and pilot-scale FCC

Supplementary Table 10. Catalyst properties for laboratory and pilot FCC experiments

Catalyst property		Data
Micro-activity		66
Specific surface area, cm^2/g		95.3
Pore volume, cm^3/g		0.028
Bulk density, g/cm^3		0.9
Particle size distribution, wt%	0 ~ 40 μm	5
	40 ~ 60 μm	23
	60 ~ 80 μm	28
	80 ~ 105 μm	23
	> 105 μm	21

Supplementary Note 18. Process conditions for laboratory-scale experiments

Supplementary Table 11. Process conditions for laboratory-scale experiments

Experiment No.	Feedstock	Temperature, ^{o}C	WHSV, h^{-1}	CTO, g/g
Test 1	Naphtha 1	460	20	7
Test 2	Naphtha 1	430	20	7
Test 3	Naphtha 1	400	20	7
Test 4	Naphtha 1	430	25	4
Test 5	Naphtha 1	430	25	7
Test 6	Naphtha 1	430	25	10
Test 7	Naphtha 1	430	15	7
Test 8	Naphtha 1	430	30	7

Supplementary Note 19. Pilot-scale reactor and experiment scheme for naphtha FCC

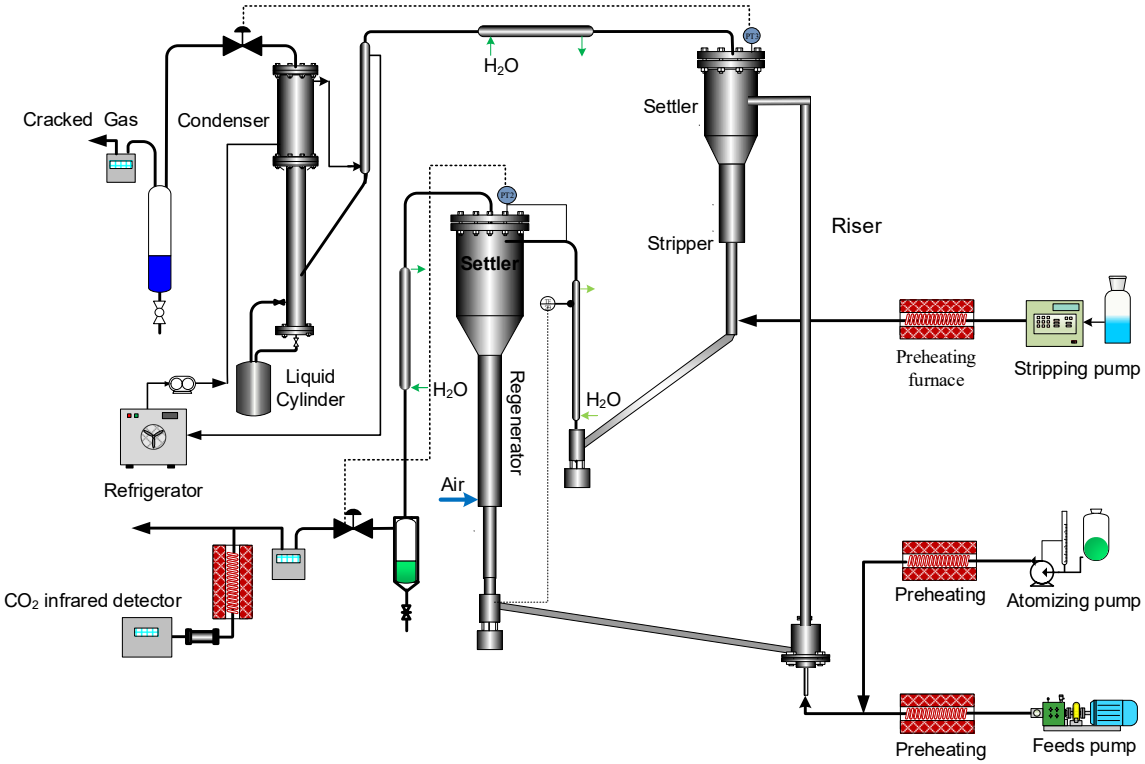

Supplementary Fig. 8. Pilot-scale reactor and experiment scheme for naphtha FCC

Supplementary Note 20. Process conditions for pilot-scale experiments

Supplementary Table 12. Process conditions for pilot-scale experiments

Experiment No.	Feedstock	Feedstock temperature, °C	Catalytic temperature, °C	Reaction time, s	CTO, g/g
Test 1	Naphtha 2	40	680	3.6	5.6
Test 2	Naphtha 2	40	640	3.6	5.6
Test 3	Naphtha 2	40	600	3.6	5.6
Test 4	Naphtha 2	40	560	3.6	5.6
Test 5	Naphtha 2	40	689	3.6	5.6
Test 6	Naphtha 2	70	678	3.6	5.6
Test 7	Naphtha 2	100	667	3.6	5.6
Test 8	Naphtha 2	200	623	3.6	5.6
Test 9	Naphtha 2	250	599	3.6	5.6
Test 10	Naphtha 2	40	680	3.6	5.8
Test 11	Naphtha 2	70	680	3.6	5.5
Test 12	Naphtha 2	100	680	3.6	5.2
Test 13	Naphtha 2	150	680	3.6	4.7
Test 14	Naphtha 2	200	680	3.6	4.1
Test 15	Naphtha 2	250	680	3.6	3.5
Test 16	Naphtha 3	200	623	3.6	5.5

Supplementary Note 21. The hyperparameter range setting in the BO algorithm

Supplementary Table 13. The hyperparameter range setting in the BO algorithm

Hyperparameter	Method	Range
Residual block number for process-based ResNet	Integer-type hyperparameters	1 ~ 2
Residual block number for molecule-based ResNet	Integer-type hyperparameters	1 ~ 2
Residual block number for integrated ResNet	Integer-type hyperparameters	1 ~ 5
Neuron number for process-based ResNet	Discrete categorical hyperparameters	128, 256, 512
Neuron number for molecule-based ResNet	Discrete categorical hyperparameters	128, 256, 512
Neuron number for integrated ResNet	Discrete categorical hyperparameters	128, 256, 512, 1024
Learning rate	Floating-point hyperparameters	0 ~ 0.5
Dropout parameter	Floating-point hyperparameters	$1.0*10^{-6}$ ~ $1.0*10^{-3}$
Weight decay	Floating-point hyperparameters	$1.0*10^{-6}$ ~ $1.0*10^{-2}$
Batch size	Discrete categorical hyperparameters	16, 32, 64, 128, 256

Supplementary Note 22. Hyperparameter range setting in the BO algorithm

Supplementary Table 14. The hyperparameter range setting in the BO algorithm

Hyperparameter	Method	Range
Learning rate	Floating-point hyperparameters	0 ~ 0.5
Dropout parameter	Floating-point hyperparameters	$1.0*10^{-6}$ ~ $1.0*10^{-3}$
Weight decay	Floating-point hyperparameters	$1.0*10^{-6}$ ~ $1.0*10^{-2}$
Batch size	Discrete categorical hyperparameters	4, 8, 16, 32, 64, 128, 256

Supplementary Note 23. Calculation process for NN-NSGA algorithm

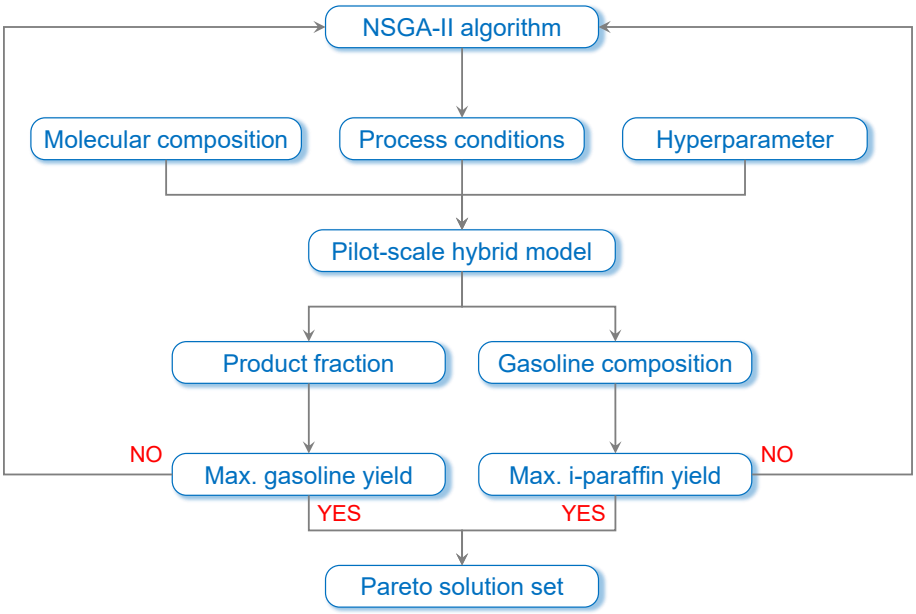

Supplementary Fig. 9. Calculation process for NN-NSGA algorithm

Supplementary Note 24. Parameters for the box plots

Supplementary Table 15. Statistical data for the box plots

	Minimum values	Maximum values	Median values	Lower limits	Upper limits	Lower whiskers	Upper whiskers
Temperature, ^{o}C	398.86	453.85	429.61	414.27	439.27	398.86	453.85
WHSV, h^{-1}	18.66	29.74	24.58	21.65	25.66	18.66	29.74
CTO	5.48	9.88	6.85	6.31	7.95	5.48	9.88
n-Paraffins, wt%	4.98	5.31	5.20	5.12	5.25	4.98	5.31
i-Paraffins, wt%	27.41	30.06	28.71	28.16	28.96	27.41	30.06
Olefins, wt%	35.93	38.39	37.11	36.88	37.79	35.93	38.39
Naphthenes, wt%	6.11	7.18	6.67	6.55	7.02	6.11	7.18
Aromatics, wt%	21.70	23.43	22.18	21.84	22.58	21.70	23.43

Supplementary Nomenclature

A = Surface Area, m^2

A_p = Effective interface heat transfer area, m^2/m^3

A_j = Arrhenius constant of reaction j

a, b, c = Adsorption parameters

α_n = Reaction index factor in the Bell-Evans-Polyani LFER of reaction family n

C_C = Coke content per unit mass of catalyst

C_i = Concentrations of species i, $kmol/m^3$

C_{pc} = Heat capacity for catalyst stream, J/(g·K)

C_{pg} = Heat capacity for oil stream, J/(g·K)

C_{ps} = Heat capacity for steam, J/(g·K)

d_c = Particle diameter for catalyst, m

Ea_j = Activation energy of reaction family j, kJ

E_{0_n} = Activation energy factor in the Bell-Evans-Polyani LFER of reaction family n

F_g = Mass flow rate for oil stream, kg/s

F_s = Mass flow rate for steam, kg/s

K_g = heat conductivity, kJ/(s·m·K)

k_j = Reaction rate constant of reaction j

K_{ads_i} = Adsorption parameter of molecule i

Mw = Average molecular weight of the oil, g/mol

m_{cat} = Mass for catalysts, g

m_{oil} = Mass for oil, g

N_{AR_i} = Number of aromatic rings of species i

N_{SC_i} = Number of saturated carbons of species i

P = Reaction pressure, kPa

P_{pc} = Pseudo-critical pressure, kPa

P_{pr} = Pseudo-reduced pressure

h_{p} = Interface heat transfer coefficient between gas and catalyst, kg/ m^2·s

R = Universal gas constant, J/mol·K

R_i = Reaction rate of species i

r_j = Reaction rate of reaction j

Sw = Weight hourly space velocity, h^{-1}

T = Reaction temperature, K

T_{c} = Temperature for catalyst stream, K

T_{g} = Temperature for oil stream, K

T_{pc} = Pseudo-critical temperature, K

T_{pr} = Pseudo-reduced temperature

v_{c} = Interstitial velocity for catalytic stream, m/s

v_{g} = Interstitial velocity for oil stream, m/s

w_{coke} = Coke mass fraction in the product

X = Reactor relative height

y_{g} = Mass fraction of oil

z = Reactor height, m

Greek letters

ΔH_j = Enthalpy of reaction j, kJ/mol

$\Delta H_{\text{vap oil}}$ = Heat of vaporization of liquid feedstock, kJ/kg

φ_{c} = Catalyst deactivation factor

ε_{c} = Volume fraction for catalyst stream

ε_{g} = Volume fraction for oil stream

μ_{g} = Viscosity for oil stream, kg/(m·s)

μ_{pr} = Pseudo-reduced viscosity

ρ_{c} = Density for catalyst stream, kg/m^3

ρ_{g} = Density for oil stream, kg/m^3

Supplementary Reference

1. Yang M*, et al.* Fischer-Tropsch wax catalytic cracking for the production of low olefin and high octane number gasoline: Experiment and molecular level kinetic modeling study. *Fuel* **303**, 121226 (2021).
2. Chen Z, Sun N, Zhang L, Wang G, Zhao S, Gao J. Molecular-Level modeling for naphtha olefin reduction in FCC subsidiary Riser: From laboratory reactor to pilot plant. *Chemical Engineering Journal* **437**, 135429 (2022).